PCCP

ROYAL SOCIETY OF CHEMISTRY

ARTICLE TYPE

Cite this: DOI: 10.1039/xxxxxxxxxx

Spatiotemporal dynamics of minimal bromate oscillators in open one-side-fed reactor†

István Molnár,[ab] Krisztina Kurin-Csörgei,[a] and István Szalai*[a]

Received Date
Accepted Date

DOI: 10.1039/xxxxxxxxxx

www.rsc.org/journalname

Minimal bromate oscillators represent the simplest version of the oscillatory reactions based on the chemistry of oxybromine species. Here, we present numerical and experimental evidences of the existence of reaction-diffusion waves in the ferroin catalyzed minimal bromate oscillator. The wave dynamics depends not only on the characteristic chemical time scales but also on that of the diffusive matter exchange which occurs between the reaction-diffusion medium and its environment. We show that the extended reactivity of ferroin catalyst towards the oxybromine species plays an essential role in the observed phenomena. In the cerium catalyzed minimal bromate oscillator the simulations support only the formation of spatial bistability.

Introduction

The oscillatory and wave phenomena observed in the Belousov-Zhabotinsky (BZ) reaction[1,2] are often regarded as the icons of far from equilibrium self-organization. The BZ reaction, which is the catalyzed oxidation of an organic substrate by bromate ions under acidic conditions, belongs to the family of bromate oscillators. A large number of variants of bromate oscillators are known. The substrate can be organic or inorganic compound, several catalysts can be used and many bromate oscillators work without catalyst.[3] The common part of the chemistry of these oscillators is the reduction of bromate to bromide ion, which includes the autocatalytic reaction between bromate and bromous acid and also the antagonistic reaction between bromous acid and bromide ion. The substrate, which is malonic acid in the classical version, typically involved in the generation of bromide ions, in the removal of the intermediate bromine and hypobromous acid and in the reduction of the oxidized form of the catalyst. To produce transient oscillations or waves in batch the substrate must perform all these tasks with appropriate rates. In a continuous-flow stirred tank reactor (CSTR) sustained dynamic phenomena can be observed under simpler chemical prerequisites. The concept of minimal oscillators is based on the idea that in an oscillatory family, a minimal set of reagents exists which are sufficient to give rise to oscillations in a CSTR.[3] A minimal bromate oscillator (MBO) consists of bromate, bromide and a catalyst, which can be cerium(IV), manganese(II), ferroin or tris(2,2'-bipyridine)ruthenium(II).[5–7]

Table 1 Core mechanism of minimal bromate oscillators[4]

	Reaction
(R1)	$BrO_3^- + Br^- + 2H^+ \rightleftharpoons HBrO_2 + HOBr$
(R2)	$HBrO_2 + + Br^- + H^+ \rightleftharpoons 2HOBr$
(R3)	$HOBr + Br^- + H^+ \rightleftharpoons Br_2 + H_2O$
(R4)	$BrO_3^- + HBrO_2 + H^+ \rightleftharpoons 2BrO_2\cdot + H_2O$
(R5)	$M^{n+} + BrO_2\cdot + H^+ \rightleftharpoons M^{(n+1)+} + HBrO_2$
(R6)	$2HBrO_2 \rightleftharpoons BrO_3^- + HOBr + H^+$

Here $M^{n+}/M^{(n+1)+}$ denotes the catalyst

These systems do not show periodic behavior in batch and have only a narrow range of oscillation in CSTR compared to the extended versions with a substrate. The appearance of oscillations in the BrO_3^-–Br^-–Ce^{4+} reaction was predicted by numerical simulations by using a six step model shown in Table 1.[8] This model represents of the simplest description of bromate oscillators. The experimental verification of the numerically predicted oscillations was realized by applying the cross-shaped phase diagram technique.[5] This technique is based on the existence of a characteristic topology for a dynamical system, in which a bistable subsystem is coupled to an appropriate feedback process.[9] Schematically, the regions of bistability and oscillations both vanish at the intersection of the stability limits of the two stable states of the system. In the CSTR experiments the input concentrations of bromate and bromide ions were used as constraints to control the state of the system and oscillations appeared around the critical point where the region of bistability disappeared.[5] The domain of oscillations in the BrO_3^-–Br^-–$[Fe(phen)_3]^{2+}$ oscillator is broader compared to the cerium catalyzed version. This corresponds to the more complex mechanism of the ferroin catalyzed system, which can be described by some additional reactions shown in Table 2.[6,10]

One of the most remarkable feature of bromate oscillators is

[a] Institute of Chemistry, Eötvös Loránd University, Budapest, Hungary. Fax: +36-1-3722592; Tel: +36-1-3722500/1902 ; E-mail: szalai.istvan@chem.elte.hu
[b] School of Ph.D. Studies, Semmelweis University, Budapest, Hungary

† Electronic Supplementary Information (ESI) available: the set of equations used in the simulations and the CSTR phase diagrams of the studied systems.

Table 2 Additional reactions for the BrO_3^-–Br^-–$[Fe(phen)_3]^{2+}$ system [10]

	Reaction
(R7)	$2\,[Fe(phen)_3]^{2+} + BrO_3^- + 3\,H^+ \longrightarrow 2\,[Fe(phen)_3]^{3+} + HBrO_2 + H_2O$
(R8)	$2\,[Fe(phen)_3]^{2+} + HBrO_2 + 2\,H^+ \longrightarrow 2\,[Fe(phen)_3]^{3+} + HOBr + H_2O$
(R9)	$2\,[Fe(phen)_3]^{2+} + HOBr + H^+ \longrightarrow 2\,[Fe(phen)_3]^{3+} + Br^- + H_2O$
(R10)	$2\,[Fe(phen)_3]^{2+} + Br_2 \longrightarrow 2\,[Fe(phen)_3]^{3+} + 2\,Br^-$
(R11)	$2\,[Fe(phen)_3]^{3+} + 2\,Br^- \longrightarrow 2\,[Fe(phen)_3]^{2+} + Br_2$
(R12)	$[Fe(phen)_3]^{3+} + Br_2 \longrightarrow [Fe(phen)_3Br_2]^{3+}$
(R13)	$Br_2 \longrightarrow Br_{2(g)}$

their capability of producing reaction-diffusion waves and patterns. [11] For this purpose the use of the ferroin/ferriin couple as a catalyst is preferred due to the distinct difference in the color of the oxidized (blue) and the reduced form (red). The BrO_3^-–$[Fe(phen)_3]^{2+}$–organic substrate type reactions are often ready to form transient reaction-diffusion phenomena under batch condition. This is a convenient feature from experimental point of view, since a simple Petri dish can be applied as a reactor. Contrary, MBOs require open reactor to operate. To study reaction-diffusion phenomena in open system all spatial points in the reactor must be fed avoiding macroscopic fluid mixing or convective transport. Thus, the feed can only be made by diffusive exchanges of chemicals with the environment. Among the different open spatial reactor designs, the so-called open one-side-fed reactor (OSFR) was successfully used to produce reaction-diffusion patterns. [12] An OSFR is typically made of an inert piece of a hydrogel which is in contact with the contents of a CSTR through a single surface. To find the conditions at which reaction-diffusion patterns can develop in an OSFR, the characteristic topology of the phase diagrams has been suggested to use. [13]

The aim of this work is to find reaction-diffusion waves using MBOs in an OSFR. Contrary to the dynamics of BZ waves, which have been explored in detail during the past decades, [14] the spatiotemporal dynamics of the core subsystem of bromate oscillators has not been examined. Although, MBOs show oscillations in a CSTR, the formation of waves in an OSFR is not trivial. In a CSTR all species are fed equally, but in an OSFR the rate of the matter exchange is different for all species, because it is determined by their individual diffusivities. Since the model prediction for the CSTR dynamics of MBOs are in quite good agreement with the experimental observations, [4] we start our investigation with numerical simulations. At this point we apply the strategy based on the cross-shaped topology of the OSFR phase diagrams. [13] The results of the simulations are tested by experiments performed in three different type of OSFRs.

Experimental and numerical methods

The experiments were performed in a thermostatted ($T = 25\,^\circ$C) OSFRs with three different gel geometries: cone, cylinder and disc (Figure 1 a-c). [15] The gel part was made of 2 w/w% agarose (Sigma A2929). The residence time in the CSTR was 100 s. The base radius (R_{base}) and the length of the cone-shape gel (l) were 1.5 mm and 27 mm, respectively. The cylinder-shape gel was made with a radius and a length of $R = 0.75$ mm and $l = 20$ mm. The disc-shape gel has a diameter $d = 24$ mm and a thickness $w = 0.75$ mm. The input flow was maintained by a peristaltic pump (Gilson minipuls 2). The feed solutions of the reactants

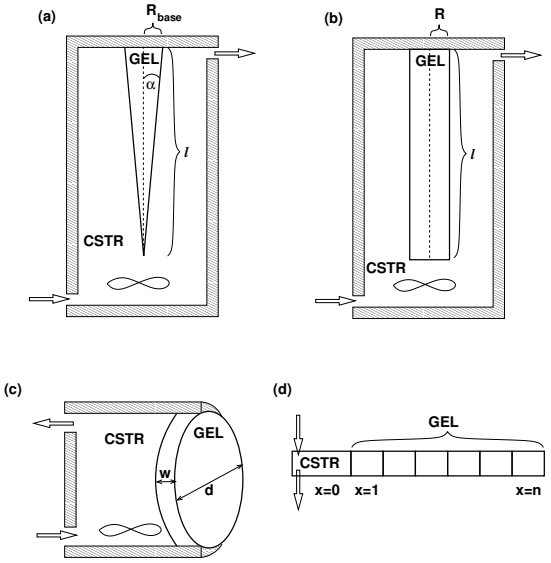

Fig. 1 Sketch of the cone (a), the cylinder (b) and the disc (c) OSFR used in the experiments and the layout of the 1D simulations (d).

were distributed in the feed tanks as follows:
Tank 1: $NaBrO_3$ (Sigma-Aldrich); Tank 2: KBr (Reanal); Tank 3: $[Fe(phen)_3]SO_4$; Tank 4: H_2SO_4 (diluted from 1.0 mol/L standard solution (Sigma-Aldrich)). All solutions were prepared with ion exchanged water and chemicals were used without further purification. The stock solution of $Fe(phen)_3]SO_4$ was prepared from a calculated amount of $[FeSO_4 \cdot 7H_2O$ (VWR) and 1,10-phenanthroline (Aldrich 99%)). The input concentration of the $[H_2SO_4]_0$ and $[Fe(phen)_3SO_4]_0$ were fixed to 0.5 M and 0.3 mM, respectively. Here, $[X]_0$ denotes the concentration that species X would have after mixing in the total inlet flow prior to any reaction. The potential changes of the CSTR content was followed with a bright platinum electrode with respect to a $Hg/Hg_2SO_4/K_2SO_4$(sat.) reference electrode connected to the CSTR via saturated K_2SO_4 salt bridge. The reactor was illuminated through a band-pass filter centered at $\lambda = 440 \pm 50$ nm and monitored by CCD camera (Imaging Source). The image processing was made by using ImageJ.

The behavior of the cerium and ferroin catalyzed MBOs are simulated by using reactions R1-R6 and R1-R13, respectively. The corresponding rate equations are shown in Table 3. A fixed concentration of H^+ is used in the simulations. The simulations of the dynamics of a 1D OSFR (Figure 1d) was made by using the next set of equations:

$$\frac{d\mathbf{c}_{\text{cstr}}}{dt} = \mathbf{f}(\mathbf{c}_{\text{cstr}}, k_1, k_2 \ldots k_n) + k_0(\mathbf{c}_0 - \mathbf{c}_{\text{cstr}}) + \rho_V \frac{\mathbf{D}}{L_x}\left[\frac{\partial \mathbf{c}}{\partial x}\right]_{x=0} \quad (1)$$

Table 3 Rate equations

$v_1 = k_1[BrO_3^-][Br^-][H^+]^2 - k_{-1}[HOBr][HBrO_2]$
$v_2 = k_2[HBrO_2][Br^-][H^+] - k_{-2}[HOBr]^2$
$v_3 = k_3[HOBr][Br^-][H^+] - k_{-3}[Br_2]$
$v_4 = k_4[BrO_3^-][HBrO_2][H^+] - k_{-4}[][BrO_2\cdot]^2$
$v_5 = k_5[M^{n+}][BrO_2\cdot][H^+] - k_{-5}[M^{(n+1)+}][HBrO_2]$
$v_6 = k_6[HBrO_2]^2 - k_{-6}[BrO_3^-][HOBr][H^+]$
$v_7 = k_7[Fe(phen)_3^{2+}][BrO_3^-][H^+]^2$
$v_8 = k_8[Fe(phen)_3^{2+}][HBrO_2][H^+]$
$v_9 = k_9[Fe(phen)_3^{2+}][HOBr]$
$v_{10} = k_{10}[Fe(phen)_3^{2+}][Br_2]$
$v_{11} = (k_{11} + k'_{11}[Br^-])[Fe(phen)_3^{3+}][Br^-]/[H^+]$
$v_{12} = k_{12}[Fe(phen)_3^{3+}][Br_2]$
$v_{13} = k_{13}[Br_2]$

and

$$\partial_t \mathbf{c} = \mathbf{f}(\mathbf{c}, k_1, k_2 \ldots k_n) + \mathbf{D}\partial_x^2 \mathbf{c} \qquad (2)$$

Dirichlet b. c. at $x = 0 (\forall y, z) : \mathbf{c}(x = 0, y, z) = \mathbf{c}_{\text{cstr}}$

No-flux boundary condition at all other gel surfaces

where $\mathbf{c}_{\text{cstr}}$ are the concentrations in the CSTR, $\mathbf{f}$ describe the kinetic functions of each species, $k_1, k_2, \ldots, k_n$ are the rate constants (Table 4), k_0 is the reciprocal residence time of the CSTR, $\mathbf{c}_0$ are the concentrations in the input flow of the CSTR, $\mathbf{D}$ is the diagonal matrix of the diffusion coefficients (Table 5), L_x is the size of the gel in the x-direction, ρ_V is the ratio between the volume of the gel and that of the CSTR and $\mathbf{c}$ are the concentrations in the gel. The last term of equation (1) can generally be neglected if $\rho_V \ll 1$. The concentrations in the CSTR provide the boundary feed composition at the CSTR/gel interface. The actual set of the equation used in the simulations can be found in the ESI.† The partial differential equations were discretized with a standard second-order finite difference scheme on a 200 mesh. The resulting systems were solved by the SUNDIALS CVODE[17] solver using the backward differentiation formula method. The absolute and the relative error tolerance were 10^{-12} and 10^{-8}, respectively.

Table 4 Rate constants

		References
$k_1 = 2\,M^{-3}s^{-1}$	$k_{-1} = 3.2\,M^{-1}s^{-1}$	16
$k_2 = 3\times10^6\,M^{-2}s^{-2}$	$k_{-2} = 2\times10^{-5}\,M^{-1}s^{-1}$	16
$k_3 = 8\times10^9\,M^{-2}s^{-3}$	$k_{-3} = 80\,s^{-1}$	16
$k_4 = 5\times10^1\,M^{-2}s^{-3}$	$k_{-4} = 4.2\times10^7\,M^{-1}s^{-1}$	16
$k_5 = 8\times10^4\,M^{-2}s^{-3}$	$k_{-5} = 8.9\times10^3\,M^{-1}s^{-1}$	16 Ce^{3+}/Ce^{4+}
$k_5 = 2\times10^9\,M^{-2}s^{-3}$	$k_{-5} = 0\,M^{-1}s^{-1}$	10 ferroin
$k_6 = 3\times10^3\,M^{-1}s^{-3}$	$k_{-6} = 1\times10^{-8}\,M^{-2}s^{-1}$	16
$k_7 = 4\times10^{-1}\,M^{-3}s^{-1}$		10
$k_8 = 2\,M^{-2}s^{-1}$		10
$k_9 = 5\times10^{-3}\,M^{-1}s^{-1}$		10
$k_{10} = 1\times10^1\,M^{-1}s^{-1}$		10
$k_{11} = 2\times10^{-4}\,s^{-1}$	$k'_{11} = 9\times10^{-3}\,M^{-1}s^{-1}$	10
$k_{12} = 5\times10^2\,M^{-1}s^{-1}$		10
$k_{13} = 1\times10^{-1}\,s^{-1}$		10

$[H_2O] = 55$ M is included in the rate constant.

Table 5 Diffusion coefficients

Species	$D/10^{-5}cm^2s^{-1}$	References
BrO_3^-	1.483	18
Br^-	2.08	18
$HBrO_2$	1.5	estimated value
HOBr	1.5	estimated value
Br_2	2.0	19
$BrO_2\cdot$	1.5	estimated value
Ce^{3+}	0.62	18
Ce^{4+}	0.62	18
$[Fe(phen)_3]^{2+}$	0.372	20
$[Fe(phen)_3]^{3+}$	0.19	20

Result and discussion

Numerical simulations

The model of the cerium catalyzed MBO (Table 1) shows bistability and oscillations in a CSTR (Figure S1 in ESI†).[8,16] The system has two stable stationary states: the F ("Flow") state has a relatively high concentration of Br^- and low concentration of Ce^{4+} ions, while the T ("Thermodynamic") state has a relatively low concentration of Br^- and high concentration of Ce^{4+} ions. When sustained reaction-diffusion phenomena are studied in an OSFR, it is reasonable to keep the CSTR content on the F state at which the extent of the overall reaction is low. In this case the gel part is fed by fresh reactants and the reactions can take place inside the gel, where two steady states, characterized by different spatial concentration profiles along the direction of the feed (axis x) can develop. The spatial steady state, at which the extent of reaction is low at all space points within the gel, is called as the F state of gel. In the other stationary state, which is called the M („mixed") state of the gel, the extent of the reaction is low at the CSTR/gel surface but turns high at the inner part of the gel.[21,22] The representative profiles of these spatial states obtained by using the cerium catalyzed MBO model are shown in Figure 2. At the M state the concentration of $HBrO_2$ significantly increases as a result of the autocatalytic process. Importantly, the concentra-

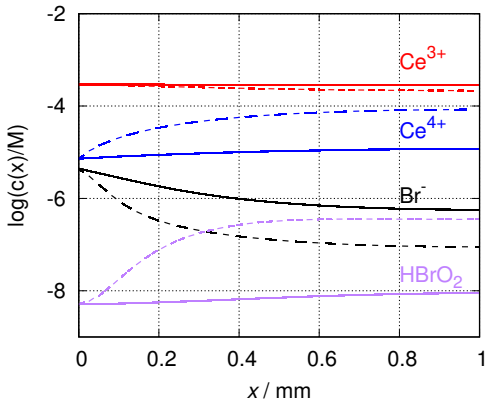

Fig. 2 Concentration profiles of the stationary states of the cerium catalyzed minimal bromate oscillator. The F and M state profiles are shown by solid and dashed lines, respectively. Parameters used in the simulation are: $k_0 = 5\times10^{-4}\,s^{-1}$, $[Ce^{3+}]_0$=0.3 mM, $[H^+]_0$=0.45 M, $[BrO_3^-]_0$=16 mM, $[Br^-]_0$=0.3 mM, $w = 1.0$ mm.

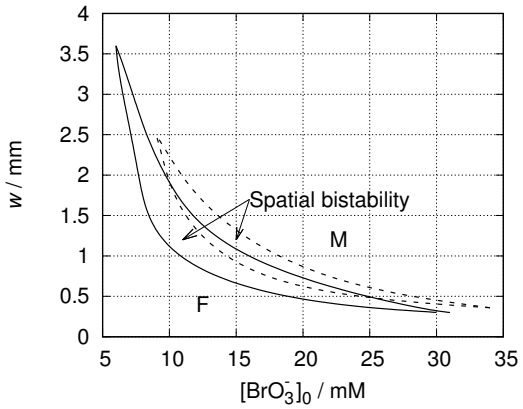

Fig. 3 Simulated OSFR phase diagram of the cerium catalyzed minimal bromate oscillator. The solid and dashed lines correspond to $[Br^-]_0$=0.2 mM and $[Br^-]_0$=0.3 mM, respectively. Parameters used in the simulation are: $k_0 = 5 \times 10^{-4}$ s^{-1}, $[Ce^{3+}]_0$=0.3 mM, $[H^+]_0$=0.45 M.

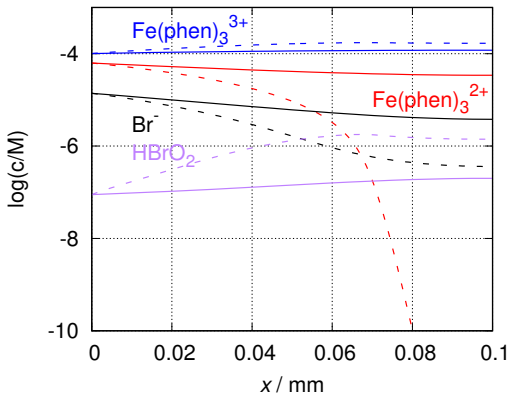

Fig. 4 Concentration profiles of the stationary spatial states of the ferroin catalyzed minimal bromate oscillator. The F and M state profiles are shown by solid and dashed lines, respectively. Parameters used in the simulation are: $k_0 = 1 \times 10^{-2}$ s^{-1}, $[Fe(phen)_3^{2+}]_0$=0.3 mM, $[H^+]_0$=0.5 M, $[BrO_3^-]_0$=12 mM, $[Br^-]_0$=0.7 mM, $w = 0.1$ mm.

tion profiles of the reduced form of the catalyst (Ce^{3+}) at the two states, do not differ considerably. The stability domains of the F and the M states overlap in the domain of spatial bistability. The size of the gel along the feeding direction, that is the thickness of the gel, is an important parameter which affects significantly the spatiotemporal dynamics of a reaction-diffusion system in an OSFR.[21,22]

To search for spatiotemporal oscillations we have checked the dynamics of the system by changing the time-scale of the diffusive matter exchange ($\tau_e \sim w^2$) between the CSTR and the gel and that of the autocatalytic process ($\tau_a \sim 1/[BrO_3^-]_0$). The F state of the gel is favored when $\tau_e < \tau_a$, e.g. at low values of w and $[BrO_3^-]_0$, while the M state is monostable when $\tau_e > \tau_a$, e.g. at high values of w and $[BrO_3^-]_0$. We found a close domain of spatial bistability in the phase diagram on the w-$[BrO_3^-]_0$ plane (Figure 3). In the domain of spatial bistability an appropriate perturbation can induce a propagating front which connects the F and the M state. To search for spatiotemporal oscillations we varied the input flow concentration of the inhibitor Br^- ion. As $[Br^-]_0$ is increased the domain of spatial bistability shrinks, but we did not find spatiotemporal oscillations. The same results were obtained by changing the other chemical parameters, like $[Ce^{3+}]_0$ and $[H^+]_0$. This result does not exclude the formation of waves in an OSFR, since the F state of the gel shows excitability which can result is the formation of a propagating pulse (Figure S2 in ESI†).

The model of the ferroin catalyzed MBO (Table 1 and 2) shows bistability and oscillations in a CSTR (Figure S3 in ESI†).[10] When the CSTR content is kept on the F state similar type of spatial steady states (F and M) can develop in the gel like in case of the cerium catalyzed MBO. There is a significant difference between the two systems, which appears in the profile of the reduced form of the catalyst at the M state. The concentration of $Fe(phen)_3^{2+}$ drops sharply inside the gel (Figure 4) and becomes practically zero ($\sim 10^{-16}$ M) at the innermost part ($x \geq 0.08$). Accordingly, the rate of reaction (R5), which is the part of the autocatalytic pathway, is also low in that region. Spatial bistability is found at relatively small thickness of the gel. Above a critical thickness

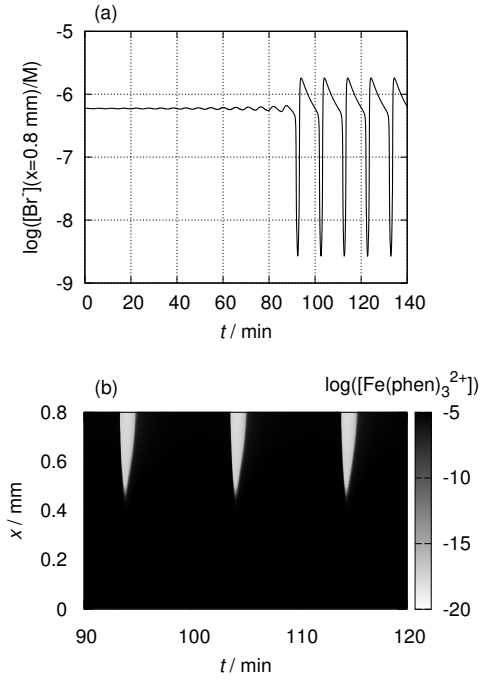

Fig. 5 Development of spatiotemporal oscillations by a transition from the F ($[BrO_3^-]_0$=23.33 mM) to the F' ($[BrO_3^-]_0$=23.34 mM) state at $t = 0$ min in the ferroin catalyzed minimal bromate oscillator (a) and the time-space plot of the oscillations (b). Parameters used in the simulation are: $k_0 = 1 \times 10^{-2}$ s^{-1}, $[Fe(phen)_3^{2+}]_0$=0.3 mM, $[H^+]_0$=0.5 M, $[Br^-]_0$=0.7 mM, $w = 0.8$ mm.

spatiotemporal oscillations develop in the gel, while the CSTR content is kept on the stationary F state. Starting from the F state of the gel by increasing $[BrO_3^-]_0$ spatiotemporal oscillations form with a finite amplitude and frequency. As a tiny region of bista-

bility between the stationary and the oscillatory state is observed, we assume the this is a subcritical Hopf bifurcation (Figure S4 in ESI†). We call this oscillatory state as F' (Figure 5). Another type

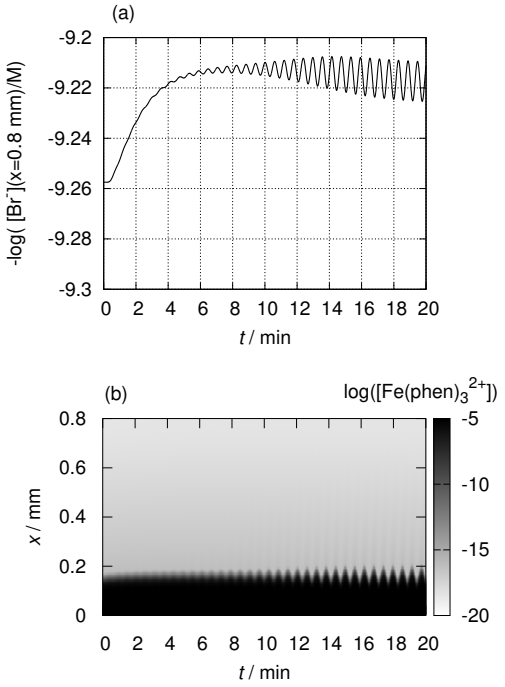

Fig. 6 Development of spatiotemporal oscillations by transition from the M ($[BrO_3^-]_0$=82 mM) to the M' ($[BrO_3^-]_0$=78 mM) state in the ferroin catalyzed minimal bromate oscillator (a) and the time-space plot of the oscillations (b). Parameters used in the simulation are: $k_0 = 1 \times 10^{-2}\,s^{-1}$, $[Fe(phen)_3^{2+}]_0$=0.3 mM, $[H^+]_0$=0.5 M, $w = 0.8$ mm.

of spatiotemporal oscillations appear through a supercritical Hopf bifurcation, when the M state of the gel becomes unstable due to the decrease of $[BrO_3^-]_0$ (Figure 6). The oscillatory M' state of the gel is characterized by low amplitude oscillations at the innermost part of the gel. The transition between the F' and M' oscillations is smooth at the parameters used in the simulations. The appearance of two different modes of spatiotemporal oscillations is not a specific phenomenon, since it has been already observed experimentally and numerically in pH-oscillators operated in an OSFR.[23–25] The phase diagram of the OSFR is again explored in the w-$[BrO_3^-]_0$ plane (Figure 7). It shows a characteristic cross-shaped topology.[9] There is a critical value of w and that of $[BrO_3^-]_0$ where spatial bistability vanishes and spatiotemporal oscillations form. The domain of spatial bistability appears below the critical w and above the critical $[BrO_3^-]_0$ and spatiotemporal oscillations develop above the critical w and below the critical $[BrO_3^-]_0$. This picture is characteristic, when a chemical negative feedback plays a significant role in the dynamics of the OSFR. The influence of the chemical negative feedback on the dynamics in the gel increases with w.[12] This effect explains the appearance of oscillations only above a critical w, when the time-scale of the matter exchange is longer than that of the inhibitory process. Among the additional reactions of the ferroin catalyzed MBO (Table 2), reaction (R13), which represents a removal of bromine, plays a crucial role. Gáspár and coworkers attributed this process mainly to the physical removal of bromine,[6] but chemical bromine consuming reaction, e.g. the bromination of the gel matrix can also play a similar role. The domain of spatiotemporal oscillations shrinks with the decrease of k_{13} (Figure S5 in ESI†) and vanishes at a certain value of k_{13}.

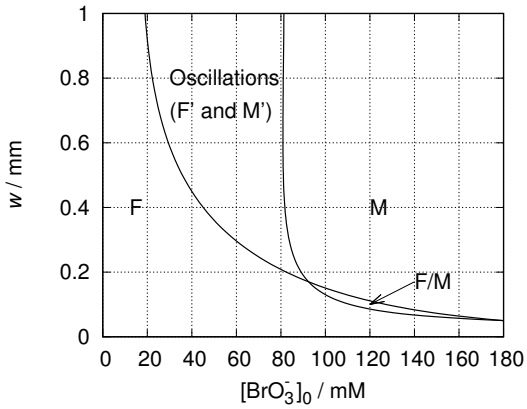

Fig. 7 Simulated OSFR phase diagram of the ferroin catalyzed minimal bromate oscillator. Parameters used in the simulation are: $k_0 = 1 \times 10^{-2}\,s^{-1}$, $[Fe(phen)_3^{2+}]_0$=0.3 mM, $[H^+]_0$=0.5 M, $[Br^-]_0$=0.7 mM.

The time-scale of the diffusive matter exchange varies with the individual diffusivities of the species. Differential diffusion can promote or depress spatiotemporal oscillations.[26] To check this effect we varied the diffusion coefficients of ferroin and ferriin by the same factor. By increasing these diffusion coefficients the oscillations vanishes at a critical level and above it spatial bistability appears (Figure S6 in ESI†). Accordingly, we can conclude that differential diffusion due to the lower diffusivities of ferroin and ferriin promotes the formation of spatiotemporal oscillations.

The results of the simulations support the development of waves in MBOs, especially in the ferroin catalyzed version, where the reactivity of ferroin provides an enhanced negative feedback.

Experimental results

To search for reaction-diffusion waves in the ferroin catalyzed MBO we used different types of OSFRs. The OSFR with a cone-shaped gel provides a convenient way to explore the effect of the thickness. The cylindrical geometry allows following the spatiotemporal dynamics along the feed direction, while with the disc geometry we can explore the quasi 2D patterns in perpendicular to the feed direction. In all experiments the CSTR is kept on the stationary F state.

First, we explored the state of the reaction-diffusion system in a cone shaped gel by increasing $[BrO_3^-]_0$. The M state appears at the base of the cone, where the thickness (the radius R) is the largest. As $[BrO_3^-]_0$ is increased the M state invades the thinner part of the cone. At $[BrO_3^-]_0$=20 mM, the tip of the M state zone starts to oscillate as it is shown in Figure 8. There are three regions in the gel (Figure 8 b). From $R = 1.5$ mm to $R = 0.6$ mm

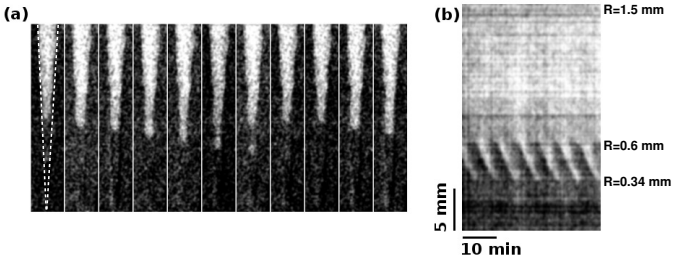

Fig. 8 Spatiotemporal oscillations in a cone-shape gel in the ferroin catalyzed minimal bromate oscillator (a) and the corresponding time-space plot made at the vertical center of the cone (b) made along the center of the cone. The sampling time of the snapshots 1 min. Experimental conditions: $[BrO_3^-]_0$=20 mM, $[Br^-]_0$=0.7 mM.

the content of the gel is in the M state. Between $R = 0.6$ mm and $R = 0.34$ mm spatiotemporal oscillations form. Below $R = 0.34$ mm the content of the gel is in the F state. The sustained oscillations are quite regular and have a period $T = 6$ min. During an oscillatory cycle the gel content oscillates between the F and the M state. According to the simulations, it is an F' type oscillations.

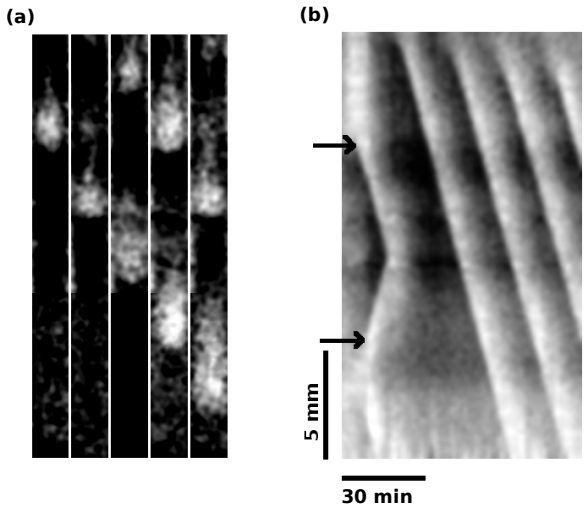

Fig. 9 Spatiotemporal oscillations in a cylinder-shape gel in the ferroin catalyzed minimal bromate oscillator (a) and the corresponding time-space plot (b) made along the vertical center of the cylinder. The sampling time of the snapshots 5 min. Experimental conditions: $[BrO_3^-]_0$=14.5 mM, $[Br^-]_0$=0.6 mM.

In the next step, we performed experiments in a cylindrical gel, where the dynamics is not influenced by the gradient of the thickness. On the base of the cone experiments we used a cylindrical gel with a radius smaller than 1 mm. At the applied conditions the gel content is in the F state below a critical $[Br^-]_0$, that is 0.6 mM. At this critical $[Br^-]_0$ at two points (marked by arrows in Figure 9b) M state regions appear in the gel. The F/M fronts start to propagate and annihilate each other when they meet. Behind the fronts the gel content returns to the F state. The next cycles start from the bottom part of the cylinder (Figure 9). A regular wave train develops with a period $T = 17$ min. The velocity of the propagating waves is $v = 1.2$ mm/min.

The use of a disc shape gel provides a new perspective. The spatiotemporal dynamics of the ferroin catalyzed MBO can be recorded in a plane parallel to the feed surface. At the conditions

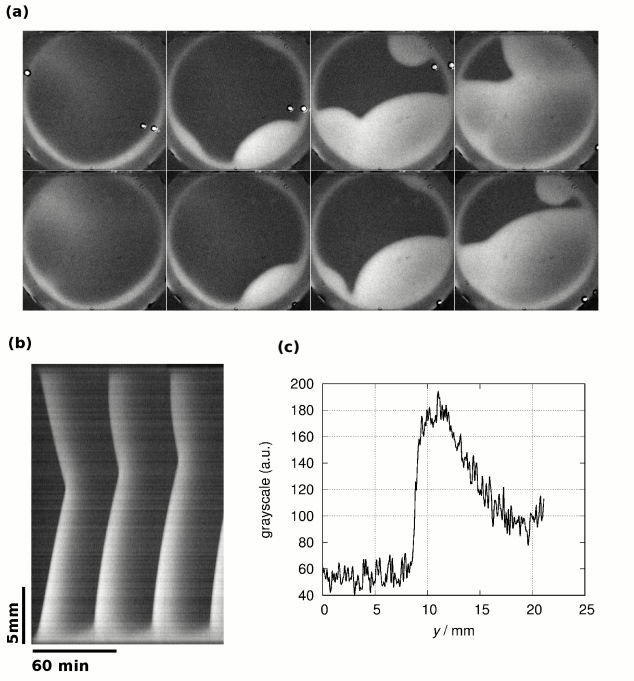

Fig. 10 Spatiotemporal oscillations in a disc-shape gel in the ferroin catalyzed minimal bromate oscillator (a), the corresponding time-space plot (b) made along the vertical diameter of the disk and the grayscale profile of the propagating wave (c). The sampling time of the snapshots 10 min. Experimental conditions: $[BrO_3^-]_0$=14 mM, $[Br^-]_0$=0.7 mM.

presented in Figure 10 the waves have a period of $T = 40$ min and a velocity of $v = 0.6$ mm/min. The waves start from pacemakers, which are randomly distributed along the rim of the disc. In the reactor a mask holds the gel tightly against an observation window, thus the part of the gel under the mask is not in contact with the content of the CSTR. This results in the appearance of pacemakers along the rim. The waves annihilate each other when they collide in the middle of the disc (Figure 10 b). The grayscale profile of the waves shows a sharp transition from the F to the M state, which is followed by a slow relaxation back to the F state (Figure 10 c).

The observed wave velocities in the ferroin catalyzed MBO are in the range of millimeters per minute, which is typical for the systems driven by the autocatalysis of $HBrO_2$.[3] However, the periods observed in our experiments are significantly larger compared to that of the BZ type systems. This corresponds to the fact that the period is mainly determined by the time scale of the relaxation from the oxidized (M) state back to reduced (F) state. In BZ systems this process is governed by the reaction between ferriin and the organic substrate. Here, in the absence of the organic substrate, in each cycle of the oscillations the gel must be refilled with ferroin by diffusion. Accordingly, the time scale of the diffusive matter exchange significantly affects the period of the spatiotemporal oscillations in the gel.

Conclusions

The simplest variants of bromate oscillators are capable to produce nontrivial spatiotemporal phenomena, like spatial bistability and waves. Numerical simulations indicate, that the formation of waves is more expected in the ferroin catalyzed MBO than in the cerium catalyzed one. This is supported by experiments, where periodic wave trains are observed in OSFRs with different geometries. The wave phenomena in a BZ type system have similar characteristics both in a batch or in an open reactor,[27] because the dynamics is mainly driven by the intermediates (e.g. Br^-, $HBrO_2$) and not by the initial reagent or input flow species (e.g. BrO_3^-, organic substrate). This is not the case in MBOs, where the role of the matter exchange is crucial. Due to the absence of the organic substrate the time scale of the relaxation from the M state to the F in an OSFR is influenced by the diffusive matter exchange. Accordingly, the spatiotemporal dynamics of the ferroin MBO bears similarities to that of the Landolt type systems.[12] This is clearly demonstrated by the formation of the F' and M' type oscillations. This work also supports the usefulness of the design method, which has been suggested to find the conditions of pattern formation in OSFRs on the basis of the typical topology of activator-inhibitor type systems.[13] We believe, that our results open the way to explore reaction-diffusion phenomena in the BZ type systems where the substrate is an inorganic compound.

Conflicts of interest

There are no conflicts to declare.

Acknowledgements

The authors thank the support of the National Research, Development and Innovation Fund (119360) and the ÚNKP-17-3 New National Excellence Program of the Ministry of Human Capacities. We thank V. Gáspar and B. Dúzs for stimulating discussions.

References

1 B. P. Belousov, *Sbornik Referatov po Radiatsionni Meditsine (in Russian)*, 1958, 145–147.
2 A. M. Zhabotinsky, *Proc. Acad. Sci. USSR*, 1964, **157**, 392–395.
3 I. R. Epstein and J. A. Pojman, *An Introduction to Nonlinear Chemical Dynamics: Oscillations, Waves, Patterns, and Chaos*, Oxford University Press, 1998.
4 K. Bar-Eli and W. Geiseler, *J. Phys. Chem.*, 1983, **87**, 3769–3774.
5 M. Orbán, P. De Kepper and I. R. Epstein, *J. Am. Chem. Soc.*, 1982, **104**, 2657–2658.
6 V. Gáspár, G. Bazsa and M. Beck, *J. Phys. Chem.*, 1985, **89**, 5495–5499.
7 T. Sekiguchi, Y. Mori, N. Okazaki and I. Hanazaki, *Chem. Phys. Lett.*, 1994, **219**, 81–85.
8 K. Bar-Eli, in *Nonlinear Phenomena in Chemical Dynamics: Proceedings of an International Conference, Bordeaux, France, September 7–11, 1981*, ed. C. Vidal and A. Pacault, Springer Berlin Heidelberg, 1981, pp. 228–239.
9 J. Boissonade and P. De Kepper, *J. Phys. Chem.*, 1980, **84**, 501–506.
10 S. Kéki, I. Magyar, M. T. Beck and V. Gáspár, *J. Phys. Chem.*, 1992, **96**, 1725–1729.
11 A. N. Zaikin and A. M. Zhabotinsky, *Nature*, 1970, **225**, 535–537.
12 I. Szalai, J. Horváth and P. De Kepper, *Chaos*, 2015, **25**, 064311.
13 J. Horváth, I. Szalai and P. De Kepper, *Science*, 2009, **324**, 772–775.
14 A. S. Mikhailov and K. Showalter, *Phys. Rep.*, 2006, **425**, 79–194.
15 P. De Kepper, J. Boissonade and I. Szalai, *Chemomechanical Instabilities in Responsive Materials*, Springer Netherlands, 2009, pp. 1–37.
16 K. Bar-Eli and R. J. Field, *J. Phys. Chem.*, 1990, **94**, 3660–3663.
17 A. C. Hindmarsh, P. N. Brown, K. E. Grant, S. L. Lee, R. Serban, D. E. Shumaker and C. S. Woodward, *ACM Trans. Math. Software*, 2005, **31**, 363–396.
18 D. Lide, *CRC Handbook of Chemistry and Physics, 86th Edition*, Taylor & Francis, 2005.
19 E. L. Cussler, *Diffusion: Mass Transfer in Fluid Systems*, Cambridge University Press, 2009.
20 G. Póta, I. Lengyel and G. Bazsa, *J. Chem. Soc., Faraday Trans. 1*, 1989, **85**, 3871–3877.
21 P. Borckmans, K. Benyaich and G. Dewel, *Int. J. Quant. Chem.*, 2004, **98**, 239–247.
22 P. Blanchedeau and J. Boissonade, *Phys. Rev. Lett.*, 1998, **81**, 5007.
23 J. Boissonade and P. De Kepper, *Phys. Chem. Chem. Phys.*, 2011, **13**, 4132–4137.
24 I. Szalai and P. De Kepper, *Phys. Chem. Chem. Phys.*, 2006, **8**, 1105–1110.
25 I. Szalai, *J. Phys. Chem. A*, 2014, **118**, 10699–10705.
26 J. Boissonade, P. De Kepper, F. Gauffre and I. Szalai, *Chaos*, 2006, **16**, 037110.
27 Z. Noszticzius, W. Horsthemke, W. McCormick, H. L. Swinney and W. Tam, *Nature*, 1987, **329**, 619–620.